Energy 37 (2012) 220–227

Contents lists available at SciVerse ScienceDirect

Energy

journal homepage: www.elsevier.com/locate/energy

Thermal effect of a thermoelectric generator on parallel microchannel heat sink

A. Rezania*, L.A. Rosendahl

Department of Energy Technology, Aalborg University, Pontoppidanstraede 101, DK-9220 Aalborg, Denmark

ARTICLE INFO

Article history:
Received 7 July 2011
Received in revised form
18 November 2011
Accepted 22 November 2011
Available online 19 December 2011

Keywords:
Thermoelectric generator
Microchannel
Geometry effect
Pumping power
Modeling
Pressure drop

ABSTRACT

Thermoelectric generators (TEG) convert heat energy to electrical power by means of semiconductor charge carriers serving as working fluid. In this work, a TEG is applied to a parallel microchannel heat sink. The effect of the inlet plenum arrangement on the laminar flow distribution in the channels is considered at a wide range of the pressure drop along the heat sink. The particular focus of this study is geometrical effect of the TEG on the heat transfer characteristics in the micro-heat sink. The hydraulic diameter of the microchannels is 270 μm, and three heat fluxes are applied on the hot surface of the TEG. By considering the maximum temperature limitation for Bi_2Te_3 material and using the microchannel heat sink for cooling down the TEG system, an optimum pumping power is achieved. The results are in a good agreement with the previous experimental and theoretical studies.

1. Introduction

In recent years, research in the field of thermo-fluids at the micro-scale level has been increased, due to the rapid growth in technological applications which require high rates of heat transfer in relatively small spaces and volumes. Many studies have been reported analytically [1,2], experimentally [3,4] and numerically [5,6] to optimize the geometrical parameters of the micro-scale heat sinks. Microchannel heat sinks that typically contain a large number of parallel microchannels with a hydraulic diameter on the order of 10 to 1000 μm have been recently applied in the automotive, chemical, food, environmental technology, aviation, and space industries [7] and thermoelectric generator (TEG) systems.

The geometric configuration of the microchannel heat sink has a critical effect on the convective heat transfer of the laminar flow in the heat sink. The laminar friction factor or flow resistance reaches a minimum value as the channel aspect ratio approaches 0.5 [8]. The laminar heat transfer increases as enlarging the hydraulic diameter or decreasing the center-to-center distance of the microchannels.

Scaling effects are often negligible in the macrochannels but may have a significant influence, and have to be counted for the microchannels [9]. The standard theories and correlations are suitable to describe heat transfer in microchannels, once cross section geometry, scaling effects and measurement uncertainties are carefully considered.

The flow and heat transfer conditions in the channels of the heat sink affect the temperature profile distribution in the N/P semiconductor materials of the TEG [10]. The small thermal conductivity of the thermoelectric materials causes the temperature difference between the cold and the hot surfaces of TEG not to vary remarkably when the mass flow rate increases in the heat sink. Due to the Seebeck effect in the TEG, which transfers a certain amount of energy from high-temperature fluid to electricity, the linear variations in temperature of the fluids in the TEG are different from the logarithmic variation case in the ordinary parallel-plate heat exchanger [6]. Therefore, the heat flow from the high-temperature fluid is not equal to the heat flow to the low temperature fluid. Crane and Jackson [11] formulated a numerical model for an integrated thermoelectric heat exchanger in a cross flow configuration with models for Bi_2Te_3 TEG. Their results show that a net power output of 1 kW can be achieved for a modestly sized heat exchanger core, to generate 45 kW/m^3 net power base on the heat exchanger volume. Optimization for a power/cost ratio objective function with a minimum net power requirement of 1 kW indicated that the power per cost can be as high as 1.1 kW/US $10,000.

A TEG system was evaluated by de Bock et al. [12] to express its performance as a function of both thermoelectric figure of merit and thermal system performance metrics, based on the derived system efficiency equations for both parallel and counter flow configurations. These equations were considered as a function of fluid inlet and outlet temperatures as well as fluid heat capacity

* Corresponding author. Tel.: +45 9940 9276; fax: +45 9815 1411.
E-mail address: alr@et.aau.dk (A. Rezania).

0360-5442/$ – see front matter © 2011 Elsevier Ltd. All rights reserved.
doi:10.1016/j.energy.2011.11.043

Nomenclature

A	TEG leg area, m^2
c	specific heat of water, 4178 J/kg K
D_h	hydraulic diameter of the channel, m
H	height, m
h	heat transfer coefficient, W/m^2 K
k	thermal conductivity, W/m K
L	length, m
$\dot{m}$	mass flow rate, kg/s
Nu	Nusselt number
P	pumping power, W
p	pressure, Pa
Pr	Prandtl number
Q	heat absorbed by coolant fluid, W
q	heat flux at the TEG hot plate, W/m^2
Re_D	Reynolds number in the channel
T	temperature, K
$\vec{V}$	velocity, m/s
W	volumetric flow rate, m^3/s
w	width, m
x_h	thermal entry length, m

Greek symbols

μ	dynamic viscosity, N s/m^2
ρ	fluid density, kg/m^3

Subscripts

al	aluminum
c	microchannel
cr	ceramic
cu	copper
f	coolant fluid
fi	coolant fluid from inlet port
fo	coolant fluid from exit
hs	heat sink
hs, w	side wall of the heat sink
s	surface of the channel
teg	thermoelectric generator
w	wall of the channel

rates and thermoelectric figure of merit. These parameters reinforced and quantified the suggestion that these parameters are crucial to the performance of TEGs. By introducing mean temperature differences between fluid streams and module sides the derived equations was observed that can be leveraged for estimating performance of more realistic systems.

There are several limiting factors in waste heat recovery systems using thermoelectric materials to achieve a high efficiency. One factor is thermoelectric conversion efficiency (electric work produced versus heat flow); another is effective heat exchanger design. Furthermore, bad system design and load matching also make the system less efficient. In TEGs, the heat sources are usually fluids or flames. Chen et al. [13] simplified the co-design and co-optimization of the TEG and a combustion system which were crucial for maximizing the system performance. A three-dimensional TEG model was proposed and the thermoelectric processes of Seebeck, Peltier, and Thomson effects were integrated with Joule source terms through a finite volume method (FVM) numerical scheme into a computational fluid dynamics simulator by FLUENT. In case of power model the greatest problem nowadays is not only the huge amount of heat dissipation, but mainly its density at the surface of the structure. Therefore, one has revealed the challenging task to design as effective heat exchanger as only possible with regard to microelectronic dimensions restrictions [14]. In order to achieve overall heat transfer enhancement a rectangular microchannel is the best shape, and its heat transfer coefficient is the highest amongst trapezoidal and triangular shaped microchannels [15]. Researches indicated that, on the basis of equal hydraulic diameter and equal Reynolds number heat sinks with rectangular channels had less thermal resistance, but required more pumping power than heat sinks with circular channels [16]. Naphon et al. [17] solved the three-dimensional governing equations for fluid flow and heat transfer characteristics using FVM. Based on the velocity distribution through a mini-rectangular fin heat sink for a CPU, the non-uniformity of the flow was observed to have a significant effect on the temperature distribution of the coolant flowing through the heat sink. Furthermore, it was found that the flow pattern at the inlet plenum has a significant effect on the velocity and direction of fluid flow at the entrance region [17]. As reported by Tuckerman and Pease [18], when the channel width and the fin thickness are equal, the heat sink gives the minimum thermal resistance. Furthermore, the convective heat transfer coefficient scales inversely with the channel width in laminar flow. Viscosity of the coolant fluid determines the minimum channel width, which gives minimum convective component of the thermal resistance.

TEGs, which convert heat energy to electrical power by means of semiconductor charge carriers serving as working fluid, have been of great interest to the energy research community in recent years. Combining the TEGs with the microchannel heat sinks gives a low weight and increases modularity of the system. Applying the microchannel to the heat sink increases the pressure drop in the heat sink in comparison with a traditional heat sink but, less flow is needed to provide the same efficiency and power in the TEG. Using microchannel heat sinks increases the Nusselt number of the channel [10]. In this work, the thermal effect of the TEG on a parallel microchannel heat sink and also the thermal reaction between them are considered and discussed. Based on the operating conditions of a real TEG, the three-dimensional governing equations for fluid flow and heat transfer were solved in the laminar flow regime by using FVM and the commercial computational fluid dynamic (CFD) solver, FLUENT. Considering the maximum temperature limitation for Bi_2Te_3 material, the thermal performance of the flow was studied along the heat sink in three heat fluxes and a wide range of pressure drops. Depending on application, component dimensions and material properties of the TEG, different heat fluxes flows across the TEG. By considering the maximum temperature limitation for Bi_2Te_3 material ($\approx$600 K) in this work, $q = 5$ W/m^2 was applied as the highest heat flux. Applying a higher heat flux caused that, the hot-side temperature of the Bi_2Te_3 material increased higher than 600 K, which was supposed to be the maximum temperature that the materials can tolerate in this work.

A symmetry boundary condition was imposed to save the computation CPU time in the system. Fig. 1a and Fig. 1b show the geometric configuration of the system and Z-cross section of the heat sink along the flow direction respectively, indicating the symmetry boundary condition. The channels being discussed are numbered in Fig. 1b.

2. Mathematical correlations

To reduce the computational effort, a symmetry boundary condition (Fig. 1) was imposed, which surrounded half of the

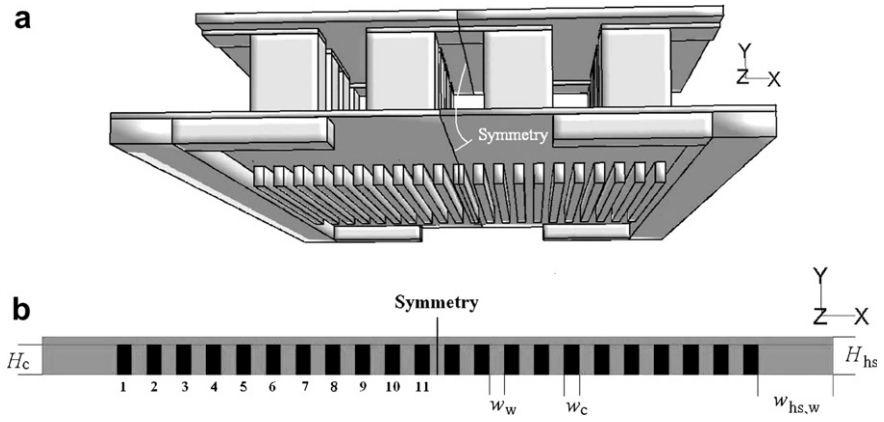

Fig. 1. a. Geometric configuration of the system, b. Z-cross section of the microchannel heat sink.

system. Since the temperature difference among the heat sink walls was low, the heat transferred by radiation was neglected. Furthermore, considering viscosity and volumetric thermal expansion coefficient of the working fluid, small channel dimensions and small temperature difference between the heat sink and the working fluid, the Grash of number (Gr) was not comparable with the Reynolds number, even at the lowest studied mass flow rate in the heat sink (Re = 3.7). The Grash of number and Reynolds number ratio was smaller than 0.01 ($Gr/Re \ll 1$) at lowest mass flow rate in current study. Therefore, the natural convection due to gravity, did not affect the flow distribution in the channels, and the fluid flow was considered under the forced convection condition in the heat sink. All the surfaces of the system exposed to the surroundings were assumed to be insulated except the hot surface of the TEG where a constant heat flux, representing the heat generation from the heat source, was specified. Therefore, based on the computational domain, the continuity, momentum and energy equations can be written in the following forms [19]:

$$\nabla \cdot \vec{V} = 0. \tag{1}$$

$$\rho_f(\vec{V}\nabla \cdot \vec{V}) = -\nabla p + \mu_f \nabla^2 \vec{V}. \tag{2}$$

$$\rho_f c(\vec{V} \cdot \nabla T) = k_f \nabla^2 T. \tag{3}$$

and for a solid region such as the TEG components, the energy equation is as follows:

$$\nabla^2 T = 0. \tag{4}$$

The heat transfer rate through the heat sink is [20]:

$$Q = \dot{m}c\left(T_{fo} - T_{fi}\right). \tag{5}$$

To produce the laminar regime in the microchannel, ten pressure drops, which are listed in Table 3, were applied to the microchannel heat sink symmetry domain. Li et al. [4] reported that transition to the turbulence regime began near Re = 1535 in microchannels. That was a Reynolds number lower than predicted by classical theory. Considering the Reynolds number and hydraulic diameter of the microchannels, $\Delta p = 50$ kPa was the maximum studied pressure drop along the heat sink in this work. On the other hand, using the low flow pressure drop decreases the pumping power in fluid systems. This pumping power is related to the pressure drop and the volumetric flow rate, and can be calculated as follows:

$$P = \Delta p W. \tag{6}$$

Therefore, the thermal characteristics of the system were also considered under the low pressure drop flows.

In a TEG, if the hot and cold junctions are maintained at different temperatures, an open-circuit electromotive force develops between them, and is given by $V = \propto \cdot \Delta T$, which defines the differential Seebeck coefficient between the two sides of the elements. Thus, the power generated is as follows [21]:

$$P = IV = V^2/R = \propto^2 \sigma \times \Delta T^2 \times A/L. \tag{7}$$

where $\propto^2 \sigma$ is the power factor.

There are two limitation factors to reduce the mass flow rate in the microchannels. One factor is the maximum temperature that a commercial sample of thermoelectric material can tolerate, and another is the maximum temperature that the water fluid can reach before evaporating. Considering these factors, $\Delta p = 0.05$ kPa was the minimum pressure drop that could be applied in the heat sink. In this study the mass flow rate range in the heat sink was between 7.83×10^{-7} kg/s at $\Delta p = 0.05$ kPa for channel #1 and 3.16×10^{-4} kg/s at $\Delta p = 50$ kPa for channel #9. The minimum and maximum Reynolds number belongs to channels #1 and #9 respectively.

Table 1
Properties of the coolant fluid and the solids used in the simulation.

Dimension	k (W/m K)					ρ (kg/m^3)	μ (kg/m s)	c_p (J/kg K)
Subscripts	f	al	cu	cr	teg	f		
Value	0.6	202.4	387.6	30	1.35	998.2	0.001	4182

Table 2
Geometry details of the system.

Parameter	Dimension
H_c (μm)	400
w_c (μm)	200
w_w (μm)	200
D_h (μm)	270
L_c (μm)	10,000
w_{hs} (μm)	10,600
H_{hs} (μm)	500
$w_{hs,w}$ (μm)	1000
H_{teg} (μm)	3000
w_{teg} (μm)	10,600
L_{teg} (μm)	10,000

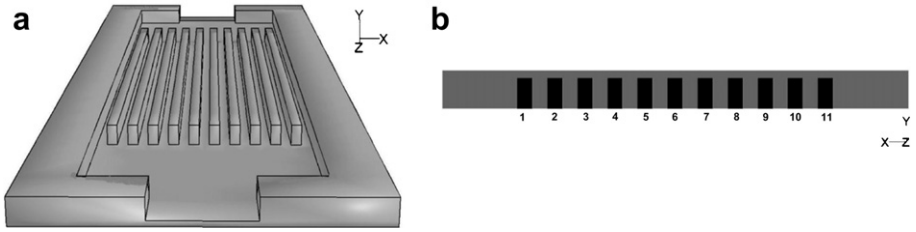

Fig. 2. a. Created geometry in order to compare the computation with [22,23], b. Z-cross sectional of the microchannel heat sink.

The thermal entry length of the internal flow at the laminar regime is approximated by [22]:

$$x_h \approx 0.05 D_h \mathrm{Re}_D \mathrm{Pr}. \tag{8}$$

The estimated thermal entry length varied between 0.36 mm in channel #1 for the minimum Reynolds number (Re = 3.7) and 144 mm in channel #9 for the maximum Reynolds number (Re = 1487). The thermal entry length was different for a constant pressure drop along the heat sink, due to the heat sink inlet arrangement. At low mass flow rate, x_h was very small. But as mass flow rate increased in the channels, due to increasing pressure drop, the effect of x_h could not be negligible. At $\Delta p = 50$ kPa, x_h was 10 times longer than the channels length, and at $\Delta p = 2$ kPa, x_h was almost equal to the length of the channels.

The local Nusselt number which is the ratio of convective to conductive heat transfer across the boundary is as follows:

$$\mathrm{Nu}(x) = \frac{h(x)D_h}{k_f} = \frac{qD_h}{k_f\left(T_s - T_f\right)} = \frac{qD_h}{k_f \Delta T_s}. \tag{9}$$

where ΔT_s is the temperature difference of the local microchannel wall temperature and the local fluid bulk temperature, and D_h is the hydraulic diameter of the microchannels defined as follows:

$$D_h = \frac{2w_c H_c}{w_c + H_c}. \tag{10}$$

Furthermore, a dimensionless temperature ratio was used for temperature comparison.

$$\mathrm{DTR} = \frac{T}{T_{\mathrm{fi}}}. \tag{11}$$

where T can be T_s and T_f. Water was used as coolant working fluid in the heat sink. The inlet fluid temperature was fixed at 293 K and three constant hot-side heat fluxes, $q = 3 \times 10^4$, 4×10^4 and 5×10^4 W/m^2, were considered to be the mass flow inlet and the wall heat flux boundary conditions, respectively.

The heat sink contained twenty two parallel microchannels and was made of aluminum. The TEG interface was copper. The thickness of the hot/cold-sides ceramic cover of the TEG was 0.2 mm and was made of a standard alumina. A commonly used, low thermal conductivity bulk thermoelectric material [23] was selected, and the dimensions of the legs of the TEG were $1.4 \times 1.4 \times 2.4$ mm. Eight TEG pairs were used in this TEG while, the distance between each leg was 0.7 mm. In Table 1, the properties of the coolant fluid and the solids used in the simulation are shown. To distribute the flow into the microchannels and collect the flow out of the microchannels, the inlet and outlet plenums with a width of 8.6 mm and a length of 6 mm were designed at the ends of the channels. These plenums can be seen in Fig. 1a. The depth of the plenums was the same as the depth of the microchannels. The area of the plenums had a width of 3.6 mm and a length of 1 mm, where the coolant working fluid entered into the plenum and exited from the plenums. Furthermore, Table 2 presents more geometry details of the system. The second-order upwind scheme was employed for spatial discretization of the main governing equations.

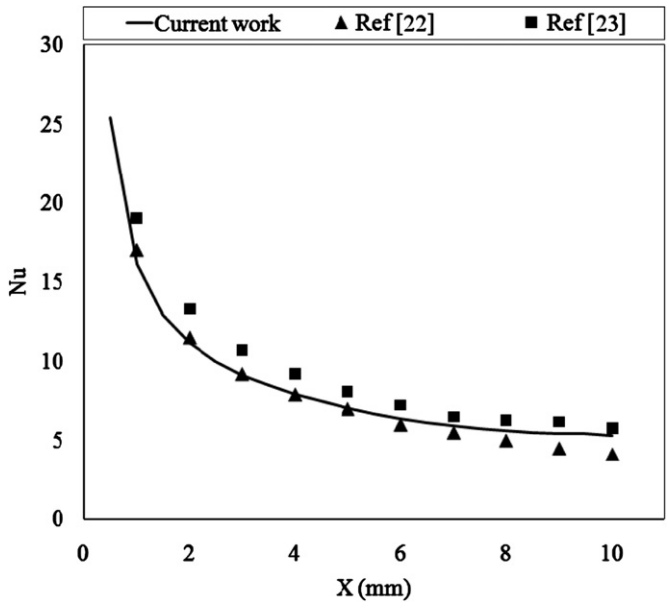

Fig. 3. Nusselt number of channel #5 compared with Refs. [22,23].

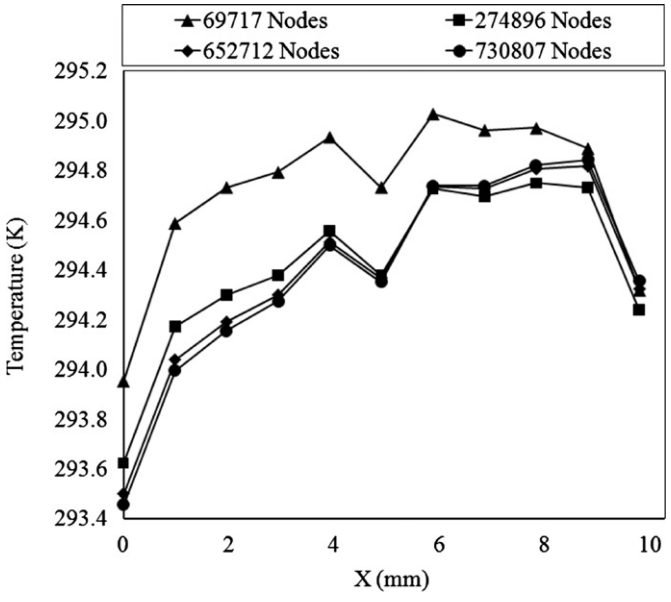

Fig. 4. Comparison of the fluid temperature at ten points along channel #2 using four different nods.

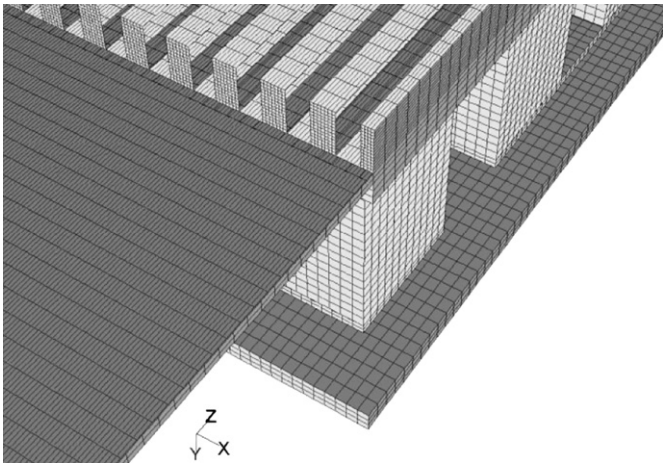

Fig. 5. Computational domain selected for the system.

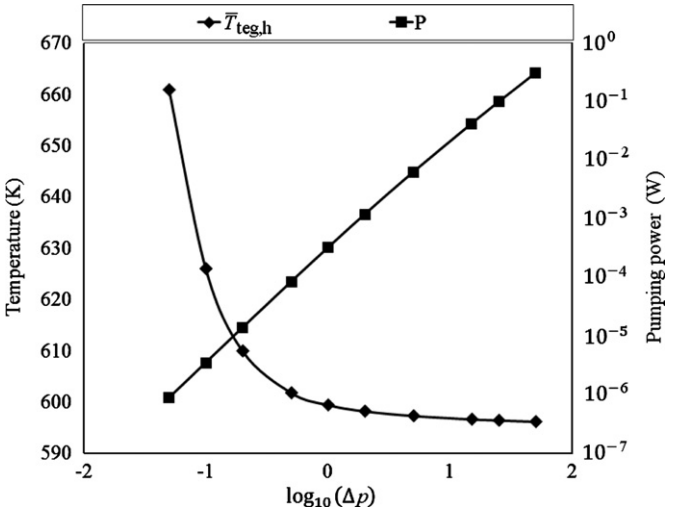

Fig. 6. Average hot surfaces of the TEG legs and the logarithm scale of the pumping power along the heat sink.

3. Validation and mesh dependency

To validate the simulation results, a new geometry (Fig. 2a) with the same geometrical characteristics in comparison with the current studied heat sink was created. Considering same boundary conditions and material properties, the Nusselt number along sample channel #5 (Fig. 2b) was compared with the computational study by Chein et al. [24] and theoretical correlation by Phillips [25]. The heat flux applied on the hot surface of the TEG was fixed at 10^6 W/m^2, and the pressure drop along the heat sink was 50 kPa. Fig. 3 shows that the simulation, computational and also the theoretical results were in a good agreement. Since the channels length was 10 mm, the heat transfer in sample channel #5 took place in thermally developing regime.

To check the domain mesh dependence of the solution, four computational domains with 69,700, 274,900, 652,700 and 730,800 nodes were tested. Fig. 4 shows the fluid temperature variations at ten points along channel #2. By considering the plots, the computational domain with 652,700 nodes was used throughout the CFD in this study. The selected computational domain of the system is shown in Fig. 5. The percentage of relative differences between the imposed heat on the hot surface of the TEG's ceramic cover and heat removed by the coolant fluid (Equation (5)) can be seen in Table 3. The percentage of the relevant differences is presented under $q = 5 \times 10^4$ W/m^2 for ten different applied pressure drops in this study. The maximum relative difference that was 4.9% belonging to $\Delta p = 50$ kPa indicated that the selected computation domain gave acceptable results.

4. Results

Base on the Fourier law, the thermoelectric materials cannot resists high heat flux, because of the resistance temperature limitation, due to the low heat conductivity. Therefore, the applied heat flux in this work was not in order of the high heat removal cooling systems such as chips in the electronic devices [2,24]. In current work, a low velocity laminar flow could remove the applied heat flux. Fig. 6 shows the average temperature of the hot surfaces ($\overline{T}_{teg,h}$) of the TEG legs and the logarithm scale of the pumping power along the heat sink in a wide range of the pressure drop at $q = 5 \times 10^4$ W/m^2. The power needed for circulating of the flow in the heat sink decreased as the pressure drop along the heat sink decreased. A pressure loss around 1 kPa could keep the $\overline{T}_{teg,h}$ under 600 K which was the temperature that could be tolerated by the thermoelectric materials [26–28]. Using a high pressure drop along the heat sink did not decrease the $\overline{T}_{teg,h}$ very much. For example, the $\overline{T}_{teg,h}$ decreased only 5.6 K (0.94%) when Δp increased 100 times from 0.5 to 50, while the pumping power decreased 3656 times (~0.3 W). Thus, considering the temperature limitation of the thermoelectric materials, a low applied pressure drop was required in the microchannel heat sink used in the TEG system.

To have a roughly comparison between the pumping power with the power generated by the TEG in the presented microchannel heat sink, a sample 2.9 × 2.9 cm^2 TEG, consists of 97 thermocouples is considered. Supposing the HZ-2 TEG [29], that can generate 7.08 W at matched load that gives 0.84 W/cm^2. The pumping power at the highest pressure drop in current study was almost equal to 0.3 W. This amount, however, was smaller than the thermoelectric power in the TEG, significantly decreased the output power generation in the system. But, at the lower pressure drops more positive electric power was achievable. The pumping power was not comparable with the generated power at the low pressure drops. As can be seen from Fig. 6, at $\Delta p = 1$ kPa the pumping power was 3.2×10^{-4} W, and was not comparable with the generated power at the low pressure drops. This point is suggested to be as the optimum applied pressure drop value, considering average temperature of the hot surfaces of the TEG legs.

In a thermal system including the TEG, the TEG's legs configuration and its thermal properties affects the temperature profile in the micro-heat sink. The surface dimensionless temperature of

Table 3
Comparison of the heat absorbed by the flow and the heat imposed on the hot surface of the TEG's ceramic cover.

Δp (kPa)	0.05	0.1	0.2	0.5	1
Q	2.677	2.677	2.677	2.677	2.675
$\lvert((Q - q \times L_{teg} \times w_{teg})/(q \times L_{teg} \times w_{teg}))\rvert \times 100\%$	1	1	1	1	0.9
Δp (kPa)	2	5	15	25	50
Q	2.670	2.678	2.678	2.653	2.52
$\lvert((Q - q \times L_{teg} \times w_{teg})/(q \times L_{teg} \times w_{teg}))\rvert \times 100\%$	0.7	1	1	0.1	4.9

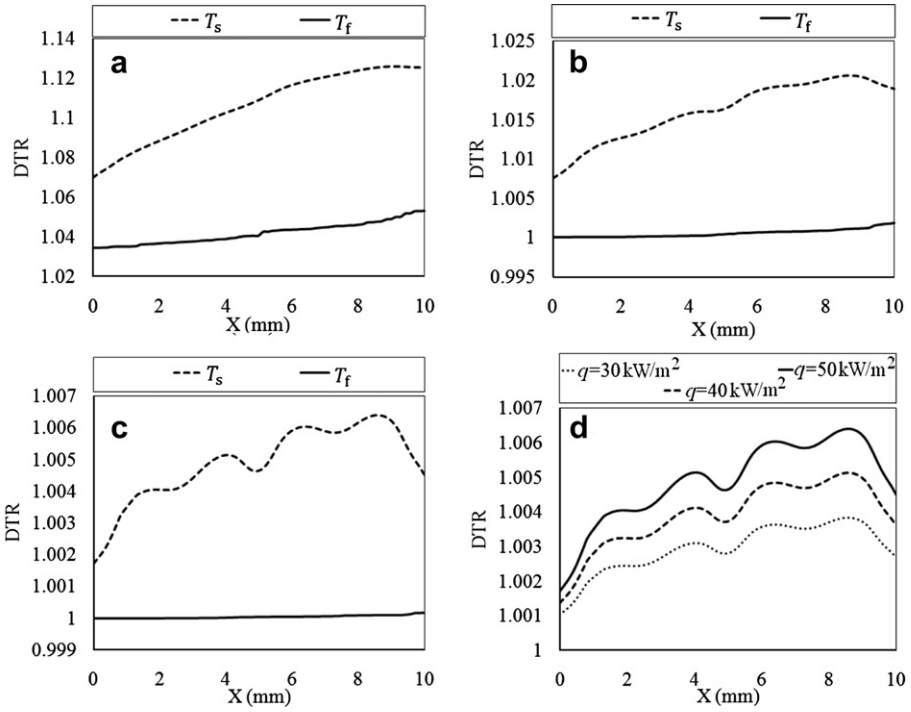

Fig. 7. Surface dimensionless temperature of channel #2, $q = 5 \times 10^4$ W/m^2. a. $\Delta p = 0.1$ kPa, b. $\Delta p = 1$ kPa, c. $\Delta p = 50$ kPa, d. different heat fluxes at $\Delta p = 50$ kPa.

sample channel #2 shown in Fig. 7a–c indicates that, when the mass flow rate was high ($\Delta p = 50$ kPa), the most crossed heat through the TEG absorbed by the coolant fluid where the legs were located. This effect caused the more fluctuating profile of the T_S plot at the higher pressure drops. A lower pumping power leads a higher thermal resistance in microchannel heat sink and vice versa [5]. When the mass flow rate decreased the heat absorbing capacity of the flow decreased, and the heat that crossed through the legs diffused in the heat sink. Therefore, the heat removal ability of the heat sink decreased at the area under the legs, and the rest region of the heat sink played a significant role to remove the applied heat flux. Thus, the temperature profile in the heat sink became almost uniform. The temperature of the coolant fluid in the channels increased more than the coolant fluid temperature at high pressure drop flows, because of absorbing a higher amount of the heat per mass flow rate ($Q/\dot{m}$) along the channel. Furthermore, Fig. 7 shows the dimensionless temperature of the flow in the channel. The surface temperature of the channel did not change along the channel as much as it changed at low pressure drop because of the high mass flow rate due to the high applied pressure drop. At the low range of the pressure drops, the temperature profile of the flow was more influenced by the legs than the

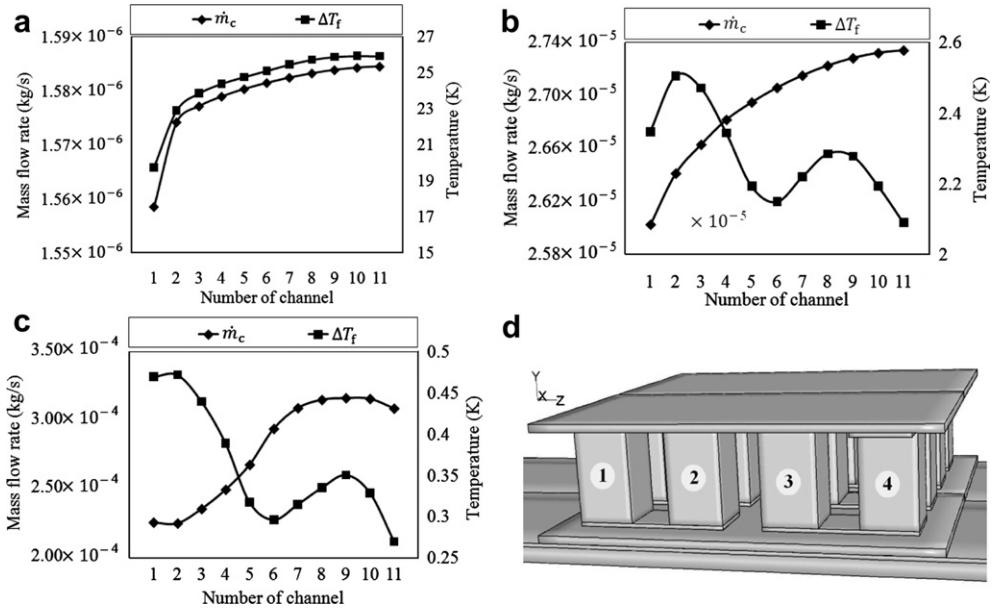

Fig. 8. Mass flow rate and the temperature difference of the coolant fluid in the channels. a. $\Delta p = 0.1$ kPa, b. $\Delta p = 2$ kPa, c. $\Delta p = 50$ kPa, d. the schematic of the TEG.

Table 4
Percentage (%) of heat removed by each channel for 3 sample pressure drops.

Δp(kPa)	Channels number										
	#1	#2	#3	#4	#5	#6	#7	#8	#9	#10	#11
0.1	7.23	8.46	8.83	9.04	9.19	9.32	9.46	9.56	9.62	9.64	9.64
1	8.74	9.66	9.63	9.31	8.90	8.79	9.00	9.19	9.18	8.95	8.65
50	9.77	9.79	9.55	8.95	7.83	8.01	8.96	9.72	10.2	9.56	7.66

temperature profile at the high pressure drops, and increased at the legs location.

At a constant pressure drop, the system showed similar thermal behavior when the applied heat flux changed. Fig. 7.d demonstrates the dimensionless wall temperature of channel #2 at $\Delta p = 50$ kPa. The temperature variation was quicker at the legs location when the applied heat flux was higher. These variations were small at the low pressure drop flows, and increased when the pressure drops increased. Fig. 8 shows the mass flow rate and the temperature difference of the coolant fluid in the microchannels for 3 sample pressure drops ($\Delta p = 0.1$, 1 and 50 kPa). The mass flow rate and the thermal distribution in the channels were affected by the arrangement of the inlet plenum and the TEG's legs, respectively. At the low pressure drops, the effect of the inlet plenum made a uniform distribution of the mass flow rate in the channels. The minimum mass flow rate was in channel #1, and the maximum flow rate was in the middle channel #11. As is mentioned, the heat diffusion in the aluminum substrate plate of the heat sink made a uniform temperature distribution on the heat convection surfaces. Therefore, the arrangement of the legs did not affect the heat transfer behavior at low mass flow rates, and the channels containing higher mass flow rate removed a higher heat, and vice versa.

Fig. 8c indicates that the arrangement effect of the legs and inlet plenum were significant in high pressure drop flows. At $\Delta p = 50$ kPa for instance, there were two picks at the temperature profile, where the microchannels were designed under the legs. As is expected, the mass flow rate in the closer channels to the edges of the heat sink were lower than the mass flow rate in the channels designed at the middle of the heat sink, as the higher pick in the temperature profile belonged to these channels. On the other hand, because channels #1, #2 and #3 were located under the legs, the temperature profile in these channels was higher than even channels #5 and #6, which were designed at the area in the heat sink between the legs. However, these channels had the higher mass flow rate. Table 4 demonstrates the percentage of the heat removed by each channel for three sample pressure drops. Considering Equation (5), the channels that were located under the legs removed higher percentage of the applied heat at high pressure drop flows.

The profiles of mass flow rate distribution in the channels changed as pressure drops varied. As can be seen in Fig. 1, the symmetry plane passed through middle of the symmetry fin. The configuration of the fin affected the distribution of the flow in the inlet plenum and channel #11, due to face to the flow perpendicularly. In this study, for the $\Delta p > 5$ kPa, the highest mass flow rate belonged to channel #10. Except channel #1, the heat transfer characteristics of the channels in the middle range of the pressure drops e.g. $\Delta p = 2$ kPa, was similar to the high pressure drop flows. As Fig. 8b shows, the inlet temperature of the flow in channel #1 was higher than the inlet temperature in the other channels. Some cooling fluid trapped at the corners of the inlet plenum, due to the plenum entrance arrangement, and its temperature increased because of the heat transferred from the plenum walls. The stationary fluid transferred the heat to the neighbor flow which entered channel #1, and increased the inlet temperature of this channel. Because of the low temperature difference between the inlet flow and the channel's walls, the removed heat was the minimum among the all channels in the heat sink.

In a TEG, the interfaces that are plated copper tabs, arrange N and P-type pellets in a TEG couple and form a junction between them. The interfaces furthermore, configure a series electrical circuit while can keep all of the heat removing in a same direction. Fig. 8d displays the interfaces and the TEG couples arrangement in this study. The interfaces that were designed between the legs and the ceramic cover plates of the TEG, affected the Nusselt number value in the channels. Because copper is a high heat conductivity material, the interfaces transferred the heat to the area between legs #1 and # 2 and also between legs #3 and #4. The interface between legs #2 and # 3 was at the top surface. The Nusselt number suddenly decreased after leg #2, because of the low heat flux on the channel surface between legs #2 and #3.

Channel #5 was designed at the area in the heat sink between the legs, and removed a lower percentage of the applied heat (Table 4). Fig. 9 illustrates that the low heat flux on the wall of channel #5 created a more uniform profile of the Nusselt number than the Nusselt number in the other channels, which are designed under two legs. Furthermore, Fig. 9 shows that, the Nusselt number at the entrance of the channels was maximum in the low mass flow rate flows, e.g., $\Delta p = 0.1$ kPa. The defused heat in the substrate of the heat sink generated an almost uniform thermal boundary layer

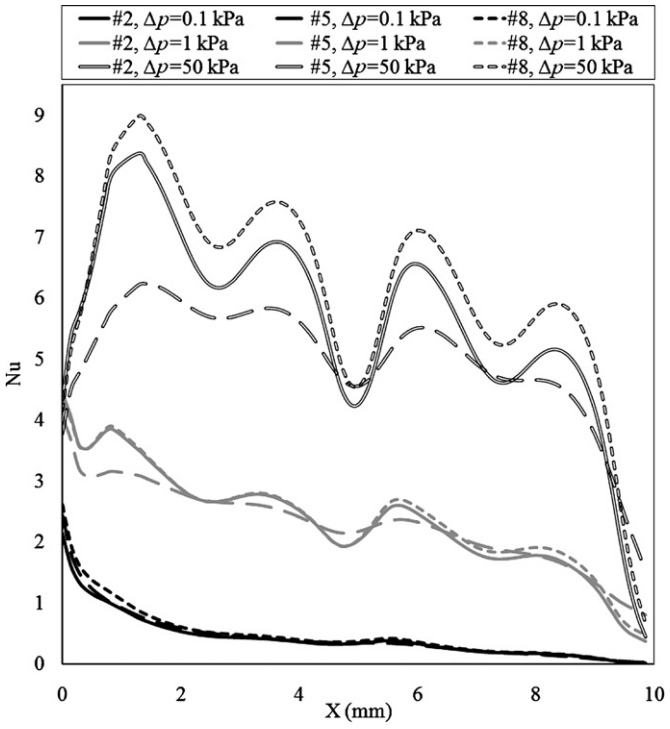

Fig. 9. Nusselt number along channel #2, $\Delta p = 50$ kPa.

in the channels, however the Nusselt number increased where the legs were located. Equation (9) indicates that, under the constant fluid heat conductivity and heat sink geometrical properties, the variation of the Nusselt number is deepened on the heat flux at the microchannel wall, the temperature difference between the local microchannel wall temperature and the local fluid bulk temperature. When the coolant fluid entered the channels from the inlet plenum, the hydraulic thickness of the fluid film and the thermal boundary layer grows along the channels. In the flow direction, the first TEG leg was located at 0.7 mm distance from the channels entrance. At high pressure drops, the thickness of the thermal boundary layer was small at the beginning of the channels, but the heat flux was low at the beginning of the channels, due to the thermal effect of the legs at the high mass flow rates. The Nusselt number was lowest along the channel, where the legs were located. When the flow along the channel reached the first leg, the crossed heat flux through the legs increased, and the Nusselt number increased quickly because of the heat flux.

5. Conclusions

The effect of the operation condition of a TEG on a parallel microchannel heat sink is considered. The three-dimensional governing equations for fluid flow and heat transfer are solved in the laminar flow regime, by using FVM. The results were generated for the detailed description of the flow and heat transfer characteristics. The effect of the location of the legs, the applied heat flux, the variation of the pressure drop along the heat sink and the arrangement of the inlet plenum were presented and discussed. As demonstrated, applying $\Delta p = 1$ kPa was sufficient to keep the thermoelectric materials under the limitation temperature (600 K). The pumping power at this optimum pressure drop was very small in comparison with the power generated by the TEG. Smaller pumping power made the system more efficient. The results showed that, as the pressure drop increases, the channels which were located under the legs removed a higher percentage of the applied heat, in comparison with the channels which, were located at the area in the heat sink between two legs. Also, the temperature of the coolant fluid increased higher in these channels than the temperature in the channels where were located at the area in the heat sink between two legs. Furthermore, the different mass flow rates in the channels, due to the inlet plenum arrangement, affected the heat transfer distribution in the microchannels. Because of the microchannels arrangement, the profile of the mass flow rate distribution in the microchannels was different at different pressure drops.

Acknowledgments

This work was carried out within the framework of the Center for Energy Materials and is funded in part by the Danish Council for Strategic Research, Programme Commission on Energy and Environment, under Grant No 823032.

References

[1] Rosa P, Karayiannis TG, Collins MW. Averaging approach for microchannel heat sinks subject to the uniform wall temperature condition. International Journal of Heat and Mass Transfer 2009;49:3447–68.
[2] Naphon P, Klangchart S, Wongwises S. Optimum thermal performance of microchannel heat sink. International Communications in Heat and Mass Transfer 2009;35:834–40.
[3] Wang BX, Peng XF. Experimental investigation on liquid forced- convection heat transfer through microchannels. International Journal of Heat and Mass Transfer 1994;37:73–82.
[4] Li H, Ewoldt R, Olsen MG. Turbulent and transitional velocity measurements in a rectangular microchannel using microscopic particle image velocimetry. Experimental Thermal and Fluid Science 2005;29:435–46.
[5] Husain A, Kim KY. Analysis and optimization of electrokinetic microchannel heat sink. International Journal of Heat and Mass Transfer 2009;52:5271–5.
[6] Yu J, Zhao H. A numerical model for thermoelectric generator with the parallel-plate heat exchanger. Journal of Power Sources 2007;172:428–34.
[7] Schubert K, Brandner J, Fichtner M, Linder G, Schygulla U, Wenka A. Microstructure devices for applications in thermal and chemical process engineering. Nanoscale and Microscale Thermophysical Engineering 2010;5: 17–39.
[8] Peng XF, Peterson GP. Convective heat transfer and flow friction for water flow in microchannel structures. International Journal of Heat and Mass Transfer 1996;39:2599–608.
[9] Rosa P, Karayiannis TG, Collins MW. Single-phase heat transfer in microchannels: the importance of scaling effects. Applied Thermal Engineering 2009;29:3447–68.
[10] Rezania A, Rosendahl LA. Evaluating thermoelectric power generation device performance using a rectangular microchannel heat sink. Journal of Electronic Materials 2011;40:481–8.
[11] Crane DT, Jackson GS. Optimization of cross flow heat exchangers. Energy Conversion and Management 2004;45:1565–82.
[12] de Bock HPJ, Novak V. Evaluation of system configurations for thermoelectric power generation, thermal and thermomechanical phenomena in electronic systems, 2008. ITHERM 2008, 11th Intersociety Conference on, 28–31 May 2008, IEEE; 2008. pp. 1276–1282.
[13] Chen M, Rosendahl LA, Condra T. A three-dimensional numerical model of thermoelectric generators in fluid power systems. International Journal of Heat and Mass Transfer 2011;54:345–55.
[14] Raj E, Lisik Z, Langer M, Tosik G, Wozny J. The numerical approach to analysis of microchannel cooling systems, ICCS 2005, LNCS 3514; 2005. 876–883.
[15] Gunnasegaran P, Mohammed HA, Shuaib NH, Saidur R. The effect of geometrical parameters on heat transfer characteristics of microchannels heat sink with different shapes. International Journal of Heat and Mass Transfer 2010;37:1078–86.
[16] Kroeker CJ, Soliman HM, Ormiston SJ. Three-dimensional thermal analysis of heat sinks with circular cooling micro-channels. International Journal of Heat and Mass Transfer 2004;47:4733–44.
[17] Naphon P, Klangchart S, Wongwises S. Numerical investigation on the heat transfer and flow in the mini-fin heat sink for CPU. International Communications in Heat and Mass Transfer 2009;36:834–40.
[18] Tuckerman DB, Pease RFW. High-performance heat sinking for VLSI. IEEE Electron Device Letters 1981;2:126–9.
[19] Chen Y, Zhang C, Shi M, Wu J. Three-dimensional numerical simulation of heat and fluid flow in noncircular microchannel heat sinks. International Communications in Heat and Mass Transfer 2009;36:917–20.
[20] Chein R, Chen Y. Performances of thermoelectric cooler integrated with microchannel heat sinks. International Journal of Refrigeration 2005;28: 828–39.
[21] Rowe DM, editor. Macro to nano. Taylor & Francis Group, LLC; 2006.
[22] Incropera FP, DeWitt DP. Fundamentals of heat and mass transfer. New York: John Wiley and Sons; 1996.
[23] Wang H, Porter WD, Sharp J. Thermal conductivity measurements of bulk thermoelectric materials, 24th international conference on thermoelectrics 2005. IEEE; 2005. 91–95.
[24] Chein R, Chen J. Numerical study of the inlet/outlet arrangement effect on microchannel heat sink performance. International Journal of Thermal Sciences 2009;48:1627–38.
[25] Phillips RJ. Microchannel heat sinks, PhD thesis. Massachusetts Institute of Technology; 1987.
[26] Borca-Tasciuc D-A, Chen G, Prieto A, Martín-González MS, Stacy A, Sands T, et al. Thermal properties of electrodeposited bismuth telluride nanowires embedded in amorphous alumina. Applied Physics Letters 2004;85:6001–3.
[27] Rosa P, Karayiannis TG, Collins MW. Thermal conductivity of Sb_2Te_3 – Gd_2Te_3 – Bi_2Te_3 solid Solutions. Inorganic Materials 2009;45:744–7.
[28] Cbung DY, Hogan T, Scbindler J, Iordanidis L, Brazis Paul, Kannewurf CR, et al. Complex bismuth chalcogenides as thermoelectrics, 16th International Conference on thermoelectrics 1997. IEEE; 1997. 459–462.
[29] Hi-Z Technology, Inc.